

**Coherence and antibunching in a trapped interacting Bose-Einstein condensate**

Shengjun Yang and Sajeev John\*

*Department of Physics, University of Toronto, 60 Saint George Street, Toronto, Ontario, Canada M5S 1A7*

(Received 7 February 2011; revised manuscript received 19 May 2011; published 13 July 2011)

We present a model for the equilibrium quantum statistics of a condensate of repulsively interacting bosons in a two-dimensional trap. Particle correlations in the ground state are treated exactly, whereas interactions with excited particles are treated in a generalized Bogoliubov mean-field theory. This leads to a fundamental physical picture for the condensation of interacting bosons through an anharmonic oscillator ground state coupled to excited Bogoliubov quasiparticles in which the quantum number statistics of condensate particles emerges self-consistently. Below the Bose-Einstein condensation temperature, our model exhibits a crossover from particle bunching to Poissonian statistics and finally antibunching as the temperature is lowered or as the trapping area is decreased. When applied to Bose condensation of long-lived dressed excitons in a photonic band gap material, our model suggests that this system may serve as a novel tunable source for nonclassical states of light.

DOI: [10.1103/PhysRevB.84.024515](https://doi.org/10.1103/PhysRevB.84.024515)

PACS number(s): 05.30.-d, 42.50.Gy, 42.70.Qs

**I. INTRODUCTION**

Bose-Einstein condensation (BEC) is a fundamental phenomena in nature and has attracted considerable attention since its prediction in 1925.<sup>1</sup> When the thermal de Broglie wavelength of massive particles becomes comparable to the interparticle spacing, quantum correlations become important. In an ideal Bose gas, a macroscopic number of particles occupy the ground state below a certain transition temperature. However, repulsive interaction must be considered to describe physical properties of both the ground state and excitation spectrum. A quantum field theoretical formulation for weakly interacting Bose condensed systems was developed by Bogoliubov.<sup>2</sup> In this mean-field theory, a complex number  $\sqrt{N_0}$  replaces the annihilation operator of the ground state, where  $N_0$  is the number of particles in an assumed coherent ground state. This mean-field decomposition allows the interacting Hamiltonian to be diagonalized and explains aspects of the elementary excitation spectra and superfluidity in weakly interacting Bose systems. However, the theory presumes coherent state formation at all temperature below the BEC transition and does not give detailed insight into the quantum statistics of particles in the condensate.

An important new research field concerns the realization of spontaneous Bose coherence of exciton-polaritons in semiconductor systems.<sup>3,4</sup> Here the effective mass of the bosons can be made many, many orders of magnitude smaller than for cold atom condensates.<sup>5,6</sup> The exciton, confined in a two-dimensional (2D) quantum well (QW), acquires its low effective mass due to strong coupling with a one-dimensional optical cavity resonance. As a result, the excitonic condensate can occur on temperature scales above 1° K. However, the strong coupling to propagating optical modes leads to a very short lifetime of the exciton due to radiative recombination. An interesting possibility is that quantum statistics of excitons can be transformed into emitted photons, when the constituent electron-hole pairs recombine by spontaneous or stimulated emission.

To understand the quantum number statistics of an excitonic condensate, the Bogoliubov model is insufficient. Two approaches, the Boltzmann equation formalism<sup>7-12</sup> and

master equation method,<sup>13,14</sup> have been used to explain the exciton-polariton distribution and coherence buildup in the nonequilibrium condensation observed in one-dimensional optical microcavity QW systems. Traditional photon lasers are based on stimulated emission of light from the excited levels of atoms when population inversion is achieved. On the other hand, exciton-polariton condensation is based on stimulated cooling of polaritons to the ground state below a critical temperature. Unlike a laser without direct photon-photon interaction, polariton-polariton scattering processes from condensed to excited polariton modes influence the coherent properties of the polariton condensate. The light emission from one-dimensional (1D) optical microcavities due to recombination in the exciton-polariton condensate has been observed to exhibit photon bunching.<sup>15</sup> On the other hand, repulsive polariton interactions are expected to suppress bunching effects due to their extra energy cost. This, in turn, facilitates coherent state formation when the system reaches thermal equilibrium. However, this has not yet been satisfied in microcavity QW systems due to very short polariton lifetimes.

In past polariton BEC experiments,<sup>3,4</sup> the lifetime of the polariton is shorter than or comparable to their phonon induced energy relaxation time. This is due to the leakage of the excitation's photonic component from the cavity due to strong coupling to radiative modes other than the cavity mode. Therefore, the polariton condensate is not in thermal equilibrium with its host lattice. With experimental advances toward BEC in semiconductor microcavities, numerous theoretical studies on the nonequilibrium steady state have been undertaken.<sup>11,12,16-19</sup> A review article on microcavity exciton-polaritons has recently appeared.<sup>20</sup> The quasi-equilibrium reached through polariton-polariton interaction is accompanied by the emission of partially coherent light. The temperature of this coherent polariton phase is not well defined. In experiments, the semiconductor microcavity is cooled down to 4 K. The threshold behavior of polariton lasing is then observed with increasing pumping power. For each pumping power, the momentum distribution of polaritons is observed and then fitted to a Bose-Einstein distribution. This

fitting temperature (around 20–50 K) is then identified with a condensate temperature, even though the system is not in thermal equilibrium.

Recently it has been suggested<sup>21,22</sup> that a new confinement mechanism for excitons in a quantum well can simultaneously achieve strong couplings to the desired optical modes as well as the long exciton lifetime. This occurs in a QW sandwiched above and below by a three-dimensional (3D) photonic band gap (PBG) material, in which the exciton radiative transition occurs very close to a photonic band edge. Strong coupling of the exciton to the zero-group-velocity band edge mode endows the exciton with the effective mass of the corresponding photon. Furthermore, vacuum Rabi splitting<sup>23</sup> of the exciton radiative recombination transition, creates two branches of the exciton dispersion relation. The lower of these two branches is pulled into the 3D photonic bandgap, where the photon that would normally be radiated by recombination forms a bound state to the exciton. This “dressed exciton” forms a dispersion minimum at the wave vector of the photonic band edge that is on the order of 10 meV below the “bare exciton” kinetic energy and which has an effective mass on the order of  $10^{-5}$  times that of bare exciton.<sup>21,22</sup> The complete confinement of light by a 3D PBG allows us to consider a limiting case of the traditional scenario involving incoherent pumping and rapid radiative decay of excitons. In our system, both the pumping rate and decay rate tend to zero and thermodynamic equilibrium is established in the exciton system.

In this paper, we construct a model for repulsively interacting Bose particles in a finite area two-dimensional trap that describes equilibrium quantum statistics of these bosons when a condensate forms below a temperature determined by (i) the depth of their dispersion minimum, (ii) their effective mass within this minimum, (iii) the trapping area, (iv) the strength of their mutual repulsion, and (v) their density within the trapping region. Our model offers a fundamental physical picture for quantum particle number statistics through a reduction of the full interacting many-body problem. This consists of a ground quantum *anharmonic* oscillator coupled to excited Bogoliubov quasiparticles. Unlike the Bogoliubov mean-field theory that treats the ground state as a simple harmonic oscillator in which coherent state formation (Poissonian number statistics) is assumed at all temperatures below the BEC transition  $T_c$ , our anharmonic oscillator model enables more general forms of quantum statistics to emerge self-consistently below the BEC transition  $T_c$ . This leads to the identification of a new temperature scale  $T_* < T_c$  below which coherence develops. As the temperature is lowered further (or the trapping area is decreased), quantum statistical properties beyond the Bogoliubov framework such as antibunching are described. While this model could apply to a general Bose condensate, we choose parameters that describe a long-lived excitonic condensate in a 3D PBG quantum well heterostructure.<sup>21,22</sup>

In Sec. II, we present a model Hamiltonian, which is divided into two parts, (i) an anharmonic ground state and (ii) excited states with dispersion. For the excited states we invoke a mean-field theory for  $\langle a_0^+ a_0^+ \rangle$  based on the exact peak position of the ground state particle number statistical distribution in the anharmonic oscillator model retained by treating particle-particle interactions exactly. This leads to an equation for the total number of particles at

thermal equilibrium. The anharmonic oscillator ground state Hamiltonian is treated exactly in Sec. III. Thermal and various Poisson-like distributions of particles in the condensate are found, depending on temperature, trapping area, and strength of exciton-exciton repulsion. We also find the coexistence of these two states for temperature very close to the BEC temperature under certain circumstances. The detailed role of excited states in the dressed-exciton dispersion, described by a depth parameter and two effective masses, is studied and elucidated in Sec. IV. Here we also determine the condensate fraction and the degree of second order coherence of the ground state for a broad range of external control parameters. Finally, a detailed analytical and numerical analysis of the ground state grand partition function is shown in the Appendix.

## II. MODEL

The general Hamiltonian for an interacting Bose system is given by

$$H = \sum_k (\epsilon_k - \mu) a_k^+ a_k + \sum_{p,q,k} \frac{1}{2} g_k a_{q+k}^+ a_{p-k}^+ a_p a_q, \quad (1)$$

where the  $a_k$  ( $a_k^+$ ) annihilates (creates) a Boson with wave vector  $k$ . Here  $\epsilon_k$  is the dressed exciton dispersion relation with a reduced effective mass minimum at the photonic band edge wave vector<sup>21,22</sup> assumed to be at  $k=0$ .  $g_k$  is a repulsive interaction. Theoretical study<sup>24</sup> has shown that electron-electron and hole-hole exchanges lead to dominant repulsive interaction among excitons, while the classical direct Coulomb interaction is negligible. The interaction typically shows a momentum cutoff of the order  $a_B^{-1}$ , where  $a_B$  is the exciton Bohr radius. For small momentum ( $k$ ), the effective repulsive bare exciton-exciton interaction energy,  $\frac{6E_b a_B^2}{S}$ , can be identified<sup>8</sup> where  $E_b$  is the bare exciton binding energy and  $S$  is the exciton confinement area. We use notation  $g_k$  for repulsive interaction and we assume a functional form  $g_k \equiv g_0 e^{-(ka_B)^2}$  and  $g_0 = \frac{6E_b a_B^2}{4S}$ . Here the additional factor of 4 in the denominator comes from the reduced repulsive interaction due to the half exciton-half photon nature of the dressed-exciton when the exciton recombination energy is in resonance with the photonic band edge. For simplicity we use this resonance form of  $g_0$  for small deviations from resonance as well. The chemical potential  $\mu$  is chosen to provide a specific number of excitons overall as determined by some external nonresonant incoherent pumping mechanism that creates these electron-hole pairs. In what follows we consider the limiting case in which the incoherent pumping rate and the exciton decay rate (radiative and nonradiative) are very small compared to the inverse equilibrium time scale. Accordingly we consider thermodynamic equilibrium of the interacting, dressed exciton system.

To describe the low temperature properties of exciton gas, we keep only the terms of the Hamiltonian (1) whose expectation values are on the order of  $\mathcal{O}(N_0)$  and  $\mathcal{O}(N_0^2)$  where  $N_0 = \langle a_0^+ a_0 \rangle$  is the ground state occupation number. We have the ground state interaction term  $a_0^+ a_0^+ a_0 a_0$  when setting all momenta  $\{p, q, k\}$  zero. We obtain  $a_0^+ a_0 a_k^+ a_k$  when setting  $\{k=0, p=0, q \neq 0\}$  or  $\{k=0, q=0, p \neq 0\}$  (direct

interaction term), and  $\{q + k = 0, p = 0, k \neq 0\}$  or  $\{p - k = 0, q = 0, k \neq 0\}$  (exchange interaction term). Finally, we retain the terms  $a_k^+ a_{-k}^+ a_0 a_0$  when  $\{p = 0, q = 0, k \neq 0\}$  (two ground state particles are scattered into two particles with opposite momentum) and  $a_0^+ a_0^+ a_k a_{-k}$  when  $\{p + k = 0, q - k = 0, k \neq 0\}$  (two particles with opposite momentum are scattered into the ground state). Equation (1) becomes

$$H \simeq \tilde{H}_0 + \tilde{H}_e, \quad (2a)$$

$$\tilde{H}_0 = (\epsilon_0 - \mu) a_0^+ a_0 + \frac{1}{2} g_0 a_0^+ a_0^+ a_0 a_0, \quad (2b)$$

$$\begin{aligned} \tilde{H}_e = & \sum_{k \neq 0} [(\epsilon_k - \mu) + (g_k + g_0) a_0^+ a_0] a_k^+ a_k \\ & + \sum_{k \neq 0} \frac{1}{2} g_k (a_k^+ a_{-k}^+ a_0 a_0 + a_0^+ a_0^+ a_k a_{-k}). \end{aligned} \quad (2c)$$

We further approximate the reduced Hamiltonian (2) using a mean-field theory for the interaction between ground state particles and excited state particles. On the other hand, we consider the full interaction between particles within the single-particle ground state manifold and we treat it as a quantum anharmonic oscillator.

In our mean-field theory we neglect any correlations between fluctuations about the assumed mean field. The absence of correlation in the fluctuation between two operators  $\hat{O}_1$  and  $\hat{O}_2$  is defined by the condition  $\langle (\hat{O}_1 - \langle \hat{O}_1 \rangle) (\hat{O}_2 - \langle \hat{O}_2 \rangle) \rangle = 0$ . In this case, the mean-field approximation of the operator product is given by  $\hat{O}_1 \hat{O}_2 \rightarrow \hat{O}_1 \langle \hat{O}_2 \rangle + \langle \hat{O}_1 \rangle \hat{O}_2 - \langle \hat{O}_1 \rangle \langle \hat{O}_2 \rangle$ . Equation (2), in this mean-field theory, becomes

$$H \rightarrow H_0 + H_e - H_{\text{const}}, \quad (3a)$$

$$\begin{aligned} H_0 = & (\epsilon_0 + I_e - \mu) a_0^+ a_0 + \frac{1}{2} g_0 a_0^+ a_0^+ a_0 a_0 \\ & + J_e (a_0 a_0 + a_0^+ a_0^+), \end{aligned} \quad (3b)$$

$$\begin{aligned} H_e = & \sum_{k \neq 0} \left\{ [\epsilon_k - \mu + (g_0 + g_k) N_0] a_k^+ a_k \right. \\ & \left. + \frac{1}{2} g_k \langle a_0 a_0 \rangle a_k^+ a_{-k}^+ + \frac{1}{2} g_k \langle a_0^+ a_0^+ \rangle a_k a_{-k} \right\}, \end{aligned} \quad (3c)$$

$$H_{\text{const}} = 2J_e \langle a_0 a_0 \rangle + I_e \langle a_0^+ a_0^+ \rangle, \quad (3d)$$

where  $I_e = \sum_{k \neq 0} (g_0 + g_k) \langle a_k^+ a_k \rangle$  and  $J_e = \frac{1}{2} \sum_{k \neq 0} g_k \langle a_k^+ a_{-k}^+ \rangle = \frac{1}{2} \sum_{k \neq 0} g_k \langle a_k a_{-k} \rangle$ . Here, both  $I_e$  and  $J_e$  may be nonzero even at zero temperature due to repulsive bosonic interactions that force some bosons to occupy single-particle excited states even when the overall system is in its many-body ground state.

The single exciton ground state energy is increased by  $I_e$  due to renormalization by excited particles. Although excited particles have a similar effect on other excited particles [included in the general Hamiltonian (1)], when performing the approximation from Hamiltonian (1) to (2) [considering the terms on the order of  $\mathcal{O}(N_0)$  and  $\mathcal{O}(N_0^2)$ ], there is no explicit term  $I_e$  in  $H_e$ . In what follows we simply absorb  $I_e$  into a redefinition of the single particle ground state energy  $\epsilon_0$ . Our mean-field theory describes spontaneous symmetry breaking in which  $\langle a_0^+ a_0^+ \rangle$  can acquire a nonzero value and a specific phase as in the conventional Bogoliubov theory.<sup>2</sup> However, unlike the standard Bogoliubov mean field in which

it is assumed that  $\langle a_0^+ \rangle = \sqrt{N_0}$  throughout, we consider a more exact treatment of bosons in the single-particle ground state manifold described by Eq. (3b). Spontaneous symmetry breaking associated with the mean-field  $\langle a_0^+ a_0^+ \rangle$  drives pair correlations of the form  $\langle a_k^+ a_{-k}^+ \rangle$  in the single-particle excited states as seen in Eq. (3c). This, in turn, leads to a coupling parameter  $J_e$  that appears in the condensate Hamiltonian (3b). In the absence of any further approximations, the Hamiltonian (3b) is analogous to that of a single-mode optical field for photons in a medium with a Kerr nonlinearity (related to  $g_0$ ) and which is parametrically amplified with photon pairs (through  $J_e$ ). It is well known in quantum optics that the Kerr effect leads to photon antibunching<sup>25</sup> and that the degenerate parametric amplifier describes quadrature squeezing<sup>25</sup> of the resulting optical field. In what follows, we consider the antibunching effects in our excitonic condensate in thermodynamic equilibrium due to repulsive interactions. For simplicity, we evaluate  $J_e$  in our mean-field theory, but use it in our ground state sector only as a justification for spontaneous symmetry breaking and phase coherence. Accordingly we take the limit of  $J_e \rightarrow 0$  in the Hamiltonian (3b) and it becomes

$$H_0 = (\epsilon_0 - \mu) a_0^+ a_0 + \frac{1}{2} g_0 a_0^+ a_0^+ a_0 a_0. \quad (4)$$

We further simplify our excited state Hamiltonian  $H_e$  by incorporating two different mean fields according to the statistical distribution of the ground state. If the peak of the ground state particle numbers distribution occurs at a nonzero particle number, we suppose coherence is built up and we choose  $\langle a_0 a_0 \rangle \approx N_0$ . In what follows, we show that this occurs at a secondary temperature scale, slightly below that required for Bose condensation. If the peak of the ground state statistical distribution occurs at zero particle number, we take  $\langle a_0 a_0 \rangle = 0$ . This occurs not only above the BEC temperature scale, but in some cases slightly below it.

*Case I: Ground state with Coherence.* The Hamiltonian of excited states, Eq. (3c), reduces to

$$\begin{aligned} H_e = & \sum_{k \neq 0} [\epsilon_k - \mu + (g_0 + g_k) N_0] a_k^+ a_k \\ & + \sum_{k \neq 0} \frac{1}{2} g_k N_0 (a_k^+ a_{-k}^+ + a_k a_{-k}). \end{aligned} \quad (5)$$

Here  $N_0$  is the expectation value of the number of particles in the ground state that, in the mean-field approximation, connects the ground state and the excited states. The Hamiltonian (5) can be diagonalized by Bogoliubov transformation

$$H_e = \sum_{k \neq 0} \epsilon_k b_k^+ b_k, \quad (6)$$

where  $b_k = \frac{a_k + \alpha_k a_{-k}^+}{\sqrt{1 - \alpha_k^2}}$ ,  $\alpha_k = \frac{\epsilon_k - \mu + (g_0 + g_k) N_0 - \epsilon_k}{g_k N_0}$ ,  $\epsilon_k = \sqrt{[\epsilon_k - \mu + (g_0 + g_k) N_0]^2 - (g_k N_0)^2}$ , and  $\epsilon_k$  is the dispersion of dressed-excitons described later by Eq. (18). The expectation value of the number of Bogoliubov elementary excitations  $\langle b_k^+ b_k \rangle = \frac{1}{e^{\beta \epsilon_k} - 1}$  where  $\beta \equiv k_B T$ . To recapture the number of excited real particles, we perform the inverse Bogoliubov transformation  $a_k = \frac{b_k - \alpha_k b_{-k}^+}{\sqrt{1 - \alpha_k^2}} = \cosh \theta_k b_k + \sinh \theta_k b_{-k}^+$ . The expectation value of the number of excited particles

$\langle a_k^+ a_k \rangle = \frac{\epsilon_k - \mu + (g_0 + g_k)N_0 - \epsilon_k}{2\epsilon_k} + \frac{\epsilon_k - \mu + (g_0 + g_k)N_0}{\epsilon_k(e^{\beta\epsilon_k} - 1)}$ . In addition, the pair correlation field  $\langle a_k^+ a_{-k}^+ \rangle = \langle \frac{b_k^+ - \alpha_k b_{-k}}{\sqrt{1 - \alpha_k^2}} \frac{b_{-k}^+ - \alpha_k b_k}{\sqrt{1 - \alpha_k^2}} \rangle = \frac{-\alpha_k}{1 - \alpha_k^2} (1 + \frac{2}{e^{\beta\epsilon_k} - 1})$ . Therefore, we can establish a pair of self-consistent equations for the chemical potential  $\mu$  and average ground state occupation  $N_0$ , for a fixed temperature and a given total number of real particles  $N$ .

The first of these equations is

$$N = N_0 + \sum_{k \neq 0} \left( \frac{\epsilon_k - \mu + (g_0 + g_k)N_0 - \epsilon_k}{2\epsilon_k} + \frac{\epsilon_k - \mu + (g_0 + g_k)N_0}{\epsilon_k(e^{\beta\epsilon_k} - 1)} \right). \quad (7)$$

The second equation is a relation between  $N_0$  and  $\mu$  obtained from an exact treatment of the condensate Hamiltonian (3b) as described in Sec. III. These two equations can be used to specify  $N_0$  and  $\mu$ .

*Case II: Ground state without Coherence.* In this case, we show that the ground state particles are still thermal distributed, although we have  $\langle N_0 \rangle \neq 0$ . Since the peak in the ground state particle number distribution appears at  $|0\rangle$ , we assume  $\langle a_0 \rangle = 0$ . The Hamiltonian of excited states is approximated by a bare boson model  $H_e = \sum_{k \neq 0} [\epsilon_k - \mu + (g_0 + g_k)N_0] a_k^+ a_k$ . The self-consistent equation for a given total number of real particles in the system is

$$N = N_0 + \sum_{k \neq 0} \frac{1}{e^{\beta[\epsilon_k - \mu + (g_0 + g_k)N_0]} - 1}. \quad (8)$$

Both cases I and II are based on a precise treatment of the ground state Hamiltonian given by Eq. (4). In the following section, we first present our evaluation of the interacting Boson partition function for this single mode. This yields the degree of second order coherence and the boson number probability distribution in the condensate. The complete results including quantum statistics of the ground state and excited states corresponding to exciton dispersion relation in a quantum well strongly coupled to photonic band edge photons<sup>21,22</sup> is presented in Sec. IV.

### III. SINGLE MODE BOSON MODEL WITH REPULSIVE INTERACTION

We consider a simple bosonic particle model with only one mode and repulsive interaction. The Hamiltonian is given by Eq. (4). This Hamiltonian is similar to that of an anharmonic oscillator describing the Kerr medium.<sup>25-27</sup> It has been shown that sub-Poissonian photon statistics emerge from a coherent laser propagating in the Kerr medium.<sup>25-27</sup> In addition, we refer the reader to Refs. 28 and 29 for an extensive discussion on the energy eigenvalue problem of the anharmonic oscillator. In this section, we apply the grand partition function to obtain the equilibrium quantum statistics of the anharmonic oscillator. We drop the mode subscript for notational simplicity. The corresponding grand partition function is

$$Z = \text{Tr} \left\{ e^{-\beta[(\epsilon_0 - \mu)a^+ a + \frac{1}{2}g a^+ a^+ a a]} \right\}. \quad (9)$$

In the particle number basis, the grand partition function (9) becomes

$$Z = \sum_n \left[ e^{-\frac{1}{2}\tilde{g}n^2 + \tilde{\mu}n} \right], \quad (10)$$

where  $\tilde{\epsilon}_0 \equiv \beta\epsilon_0$ ,  $\tilde{\mu} \equiv \beta\mu$ ,  $\tilde{g} \equiv \beta g$ , and  $\tilde{\epsilon}_0 - \frac{1}{2}\tilde{g} \equiv 0$ .

The probability to occupy the number state  $|n\rangle$  is

$$P(n) = \frac{1}{Z} e^{\tilde{\mu}n - \frac{1}{2}\tilde{g}n^2}. \quad (11)$$

When  $\tilde{\mu} < 0$ , the probability decreases monotonically with  $n$  and its distribution is similar to the thermal distribution of noninteracting bosons. When  $\tilde{\mu} > 0$ , the probability increases first and then decreases with  $n$ , with a peak for occupying  $|n \neq 0\rangle$ . The sign of the chemical potential characterizes a fundamental difference in quantum statistics of the condensate.

Through our derivation in the Appendix, the value of the grand partition function is given by

$$Z = \begin{cases} Z_n & : \tilde{\mu} < 0, \\ Z_n + Z_s & : \tilde{\mu} > 0, \end{cases} \quad (12a)$$

$$Z_n \simeq Z_A = e^{\frac{1}{2}\tilde{g}x_0^2 + \ln[1+x_0]} [1 + \tilde{g}x_0(1+x_0)]^{-1/2}, \quad (12b)$$

$$Z_s = \sqrt{\frac{\tilde{g}}{2\pi}} e^{\frac{1}{2}\frac{\tilde{\mu}^2}{\tilde{g}} - \frac{2\pi}{\tilde{g}}}, \quad (12c)$$

where  $Z_A$  is obtained under a saddle point approximation when evaluating Eq. (A5b) and  $x_0$  is the saddle point described by Eq. (A4). With this analytical evaluation of grand partition function, it is straightforward to find the expectation value of the number of particles in the ground state by  $\langle N_0 \rangle = \frac{\partial}{\partial \tilde{\mu}} \ln Z$ , which is described by Eqs. (A9).

For a given average particle number  $\langle N_0 \rangle$  in the ground state, we can solve for  $x_0$  in Eqs. (A9) and obtain the chemical potential through the relation (A4). This yields the probability distribution of bosons (11) in the ground state. The degree of second order coherence<sup>25</sup> is given by

$$I_{\text{sec}} \equiv \frac{\langle a^+ a^+ a a \rangle}{\langle a^+ a \rangle^2} = \frac{\langle N_0^2 \rangle - \langle N_0 \rangle}{\langle N_0 \rangle^2}. \quad (13)$$

Using  $\langle N_0^2 \rangle = \frac{1}{Z} \frac{\partial^2 Z}{\partial \tilde{\mu}^2} = \langle N_0 \rangle^2 + \frac{\partial \langle N_0 \rangle}{\partial \tilde{\mu}}$ , this becomes

$$I_{\text{sec}} = 1 + \frac{1}{\langle N_0 \rangle^2} \left( \frac{\partial \langle N_0 \rangle}{\partial \tilde{\mu}} - \langle N_0 \rangle \right). \quad (14)$$

It follows from Eq. (A9) in the Appendix that we have the analytical expression of  $\frac{\partial \langle N_0 \rangle}{\partial \tilde{\mu}}$  given by Eqs. (A10).

In Fig. 1(a), three curves with circle dots (blue online) are solutions of Eq. (A9a) with a positive chemical potential for three different values of  $\langle N_0 \rangle$ . As  $\tilde{g}$  increases  $\frac{x_0}{\langle N_0 \rangle}$  approaches unity. The corresponding second order coherence in Fig. 1(b) shown by three lines with triangle dots (green online) decreases from large positive values to values below 1, indicating a crossover from dressed-exciton bunching to antibunching as the repulsive interaction increases. This corresponds to a change from super-Poissonian to Poissonian and then to sub-Poissonian dressed-exciton number distribution. The three red curves with plus (+) dots are solutions of Eq. (A9a) with a negative chemical potential. As  $\tilde{g}$  decreases  $\frac{x_0}{\langle N_0 \rangle}$  again approaches unity. The corresponding degrees of second order

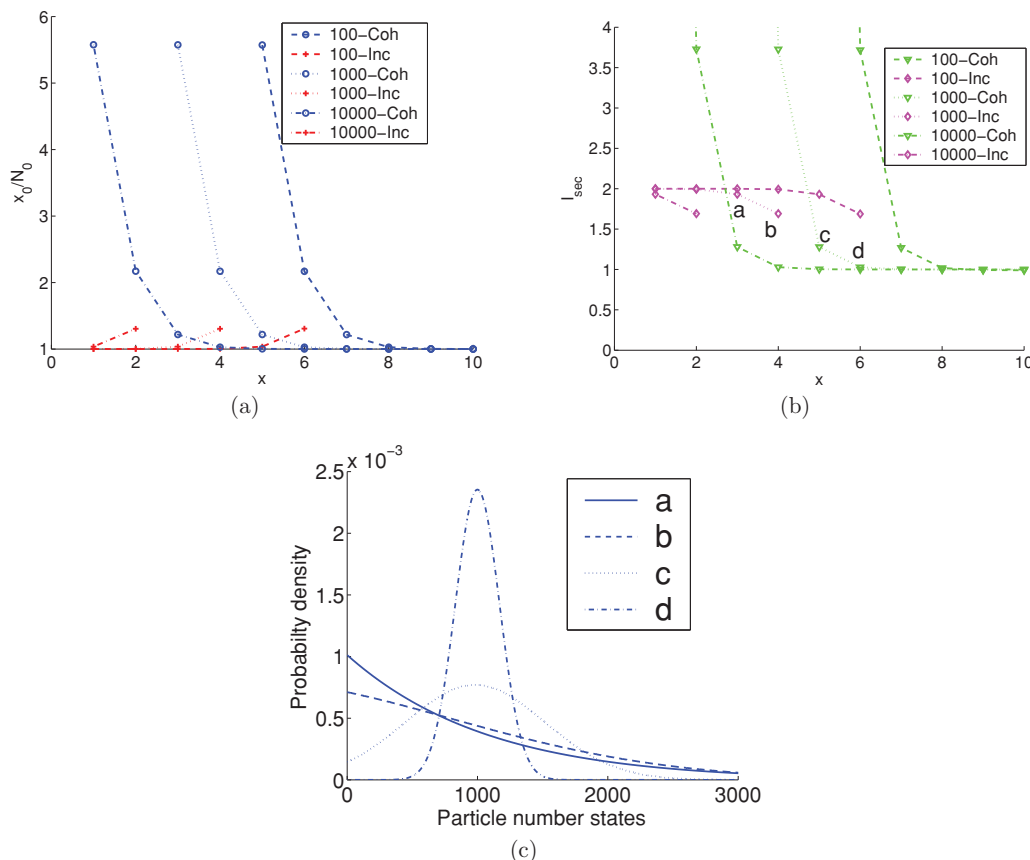


FIG. 1. (Color online) (a) The value of  $\frac{x_0}{N_0}$  is shown as a function of  $\tilde{g}$  for the single mode interacting Boson model with three different choices of  $N_0 = 100, 1000, 10000$ , where  $x = (\ln \tilde{g})/2.3026 + 10.4583$ . The *Coh* in the legend denotes the branch of the solution from Eq. (A9a) with a positive chemical potential because partial coherence is built up in this branch. The *Inc* in the legend denotes the branch of the solution from the Eq. (A9a) with a negative chemical potential due to the incoherent statistical nature of bosons in this branch. (b) The corresponding degree of second order coherence for each solution in (a) is shown. (c) Statistical distributions for four specific points indicated by *a, b, c, d* are shown. These four points have the same  $\langle N_0 \rangle = 1000$ , but with different  $\tilde{g}$  from weak to strong. The corresponding  $x$  values for  $\tilde{g}$  are 3, 4, 5, 6 for *a, b, c, d*, respectively.

coherence in Fig. 1(b) shown by three lines with diamond dots (magenta online) increase from a value larger than unity to a limiting value of 2 for an ideal Bose thermal distribution. We note that the saddle point  $x_0$  converges to the number of ground state particles  $\langle N_0 \rangle$  for either strong or weak  $\tilde{g}$ . When the chemical potential is positive, we also observe that for fixed  $\tilde{g}$  there will be smaller ratio of  $\frac{x_0}{N_0}$  for larger  $N_0$ . This corresponds to the smaller value of the degree of second order coherence and suppressed fluctuation in the ground state when the number of particles is greater.

The variation in exciton number distribution for four different choices of  $\tilde{g} = 0.3481 \cdot 10^{x-10}$ ,  $x = 3, 4, 5, 6$  with the same  $\langle N_0 \rangle = 1000$  for *a, b, c, d* points are shown in Fig. 1(c). As the statistical distribution changes from the super-Poissonian to sub-Poissonian by either (i) lowering the temperature, (ii) decreasing the trap size, dressed-exciton antibunching occurs. It is of considerable importance if this antibunching in the condensed dressed excitons system can directly be transferred to the statistics of light emitted by the radiative recombination of the underlying electron-hole pairs. The light for which the photons arrive at regular time intervals has a lower photon-number fluctuation than the other light with statistically independent photon arrival times. This

“shot” noise limits the accuracy with which information can be transmitted by small numbers of photons. Antibunched light from our dressed exciton condensate may provide an important alternative to conventional laser light for low noise measurements and information transfer.

As shown in Fig. 1(a),  $x_0$  approaches  $N_0$  both at very low and very high temperatures. By approximating  $x_0 \approx N_0$ , the chemical potential becomes  $\tilde{\mu} \approx \tilde{g}N_0 - \ln(1 + N_0^{-1}) = \tilde{g}N_0 - N_0^{-1} = (\tilde{g}N_0^2 - 1) \cdot N_0^{-1}$ , for  $N_0 \gg 1$ . This is true whenever there is macroscopic occupation of the ground state. Therefore, the sign of  $\tilde{\mu}$  is determined by the value of  $\tilde{g}N_0^2$  relative to unity, (i.e.,  $\tilde{\mu} > 0$  when  $\tilde{g}N_0^2 > 1$  and  $\tilde{\mu} < 0$  when  $\tilde{g}N_0^2 < 1$ ). The probability distribution for the number of excitons in the ground state follows from the Eq. (11)

$$P(n) = \frac{1}{Z} e^{-\frac{1}{2}\tilde{g}(n-\frac{\tilde{\mu}}{\tilde{g}})^2 + \frac{\tilde{\mu}^2}{2\tilde{g}}}. \quad (15)$$

If  $\tilde{\mu} \gg \tilde{g}^{0.5}$ , the distribution approaches the Gaussian probability density function  $\frac{1}{\sqrt{2\pi\sigma^2}} \exp(-\frac{(n-\bar{n})^2}{2\sigma^2})$  with  $\bar{n} = \tilde{\mu}/\tilde{g}$  and  $\sigma = \tilde{g}^{-0.5}$ . Figure 2 shows the degree of second order coherence as a function of  $\tilde{\mu}$  with the expectation value  $\langle n \rangle = 1000$  of the distribution described by Eq. (15). The

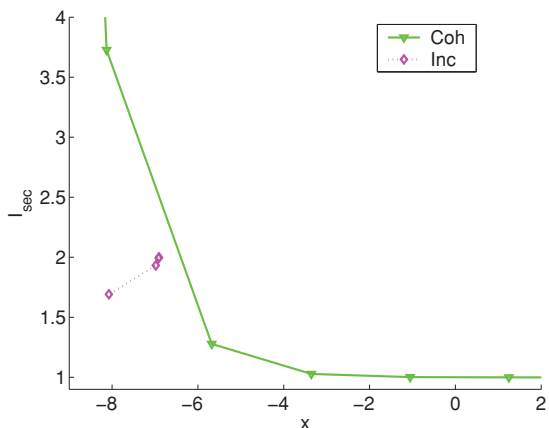


FIG. 2. (Color online) The degree of second order coherence as a function of  $\tilde{\mu}$  with the expectation value  $\langle n \rangle = 1000$  of the distribution described by Eq. (15). The solid curve is the branch for positive  $\tilde{\mu}$  with  $x = \ln \tilde{\mu}$  denoted by *Coh*. The dotted curve is the branch for negative  $\tilde{\mu}$  with  $x = \ln(-\tilde{\mu})$  denoted by *Inc*.

dotted curve indicates a slight coherence buildup from the thermal distribution ( $I_{\text{sec}} = 2$ ) when the negative chemical potential increases toward zero (i.e., the left direction of the  $x$  axis). However, the solid curve shows a much larger  $I_{\text{sec}}$ , that is, a large number fluctuation, for smaller positive chemical potential, and the degree of second order coherence decreases toward the value slightly less than unity (the right direction of the  $x$  axis).

#### IV. EXCITON CONDENSATION NEAR A PHOTONIC BAND EDGE

##### A. BEC temperature in a 2D finite system

In an infinite 2D system, BEC occurs only at zero temperature due to low energy, long wavelength, phase fluctuations for temperature  $T > 0$ . However, a confinement potential can discretize the system energy spectrum, allowing BEC to occur at finite temperature. Here, we consider the macroscopic occupation of the ground state as evidence for BEC without going to the thermodynamic limit (i.e., the confinement area  $S$  is finite). For an ideal Bose gas in a finite system, the energy spectrum  $E_i$  ( $i = 0, 1, 2, \dots$ ) is discrete and  $E_0 = 0$  denotes the ground state. The expectation value of number of particles is  $N = N_0 + N_e$ , where  $N_0 = (z^{-1} - 1)^{-1}$  and  $z \equiv e^{\beta\mu}$  is the fugacity. The number of excited particles is

$$N_e = \sum_{i=1}^{\infty} \frac{1}{z^{-1} e^{E_i/k_B T} - 1}. \quad (16)$$

We have  $1/z = 1 + 1/N_0 \approx 1$  for  $N_0 \gg 1$  whenever a macroscopic occupation of the ground state occurs, otherwise  $N_0$  is negligible and  $N_e \approx N$ . Therefore, as temperature decreases,  $z$  (determined by  $N$  and  $T$ ) approaches unity and a macroscopic number  $N_0$  appears. We define a reference critical temperature  $T_c$  (Ref. 30) to characterize this crossover

$$\sum_{i=1}^{\infty} \frac{1}{e^{E_i/k_B T_c} - 1} = N. \quad (17)$$

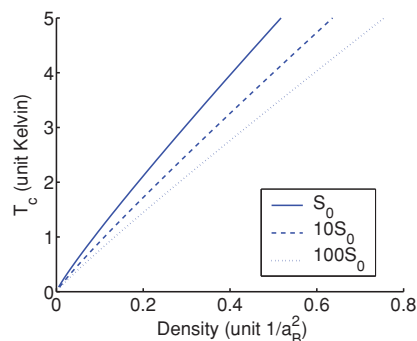


FIG. 3. (Color online) The critical (reference) temperature  $T_c$  as a function of the particle density.  $T_c$  is defined by Eq. (17) with the assumption of zero occupation of the ground state. Here, there is no coupling to band edge photons and we use the bare exciton ( $m_{\text{exc}} = 0.57m_e$ ). Depicted are three different choices of the exciton confinement area. Here  $S_0 = (10 \mu\text{m})^2$  and  $m_e$  is bare electron mass.

In what follows, we associate  $T_c$  with the BEC transition temperature for a finite size system.

In general the energy spectrum for a 2D box with area  $S$  is  $E_{n_x, n_y} = \frac{\hbar^2 \pi^2 (n_x^2 + n_y^2)}{2mS}$  ( $n_x$  and  $n_y$  are positive integers). In our description of the reference temperature, the ground state energy  $E_{1,1}$  is redefined as the zero of energy. When transforming the summation (17) into an integral, the range of integration is from the first excited states  $E_{1,2}$  to infinity.

Figure 3 shows the critical temperature  $T_c$  as a function of the particle density with effective mass  $m_{\text{exc}} = 0.57m_e$  (no dressing by photons) and various confinement areas. The critical transition temperature is on the order of Kelvin for the exciton density below unity per Bohr radius square. On the other hand, if we consider ultramobile dressed excitons in a PBG QW heterostructure with a simple parabolic dispersion for *all* energies, the effective-mass model would predict a critical temperature on the order of thousands of degrees Kelvin. This is due to the very low effective mass in the dressed exciton dispersion minimum relative to that of the bare exciton. This temperature scale is far beyond the range of validity of the single effective mass model.

To achieve a realistic estimate of the BEC critical temperature, it is necessary to consider a more detailed dispersion curve (see Fig. 4) characterized by three parameters (i) the photon effective mass in the dispersion minimum, (ii) the depth of the dispersion minimum, and (iii) the bare exciton effective mass valid for wave vectors away from the photonic band edge and energies higher than the dressed exciton dispersion minimum. Strong exciton dressing occurs only at the wave vector corresponding to a photonic band edge, when the exciton radiative recombination energy coincides with the band edge energy. The full dressed exciton dispersion curve is similar to that of an exciton-polariton in semiconductor microcavity. Accordingly, we model the dressed exciton dispersion as

$$\epsilon_k = \frac{E_{\text{exc},k} + E_{\text{ph},k} - \sqrt{(E_{\text{exc},k} - E_{\text{ph},k})^2 + 4(\hbar g_{xp})^2}}{2} + \hbar g_{xp}. \quad (18)$$

Here  $m_{\text{exc}}$  and  $m_{\text{ph}}$  are the bare exciton effective mass and photon effective mass at a photonic band edge. Also

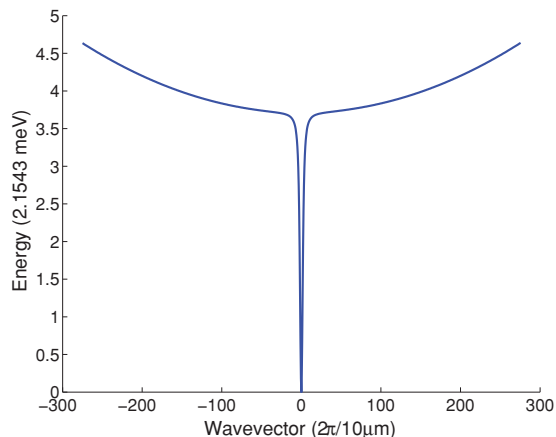


FIG. 4. (Color online) The dispersion curve described by Eq. (18) for an exciton strongly coupled to band edge photons. Here the bare exciton effective-mass  $m_{\text{exc}} = 0.57m_e$ , the band edge photon effective-mass  $m_{\text{ph}} = 5.7 \times 10^{-6}m_e$ , and the exciton-photon coupling  $g_{xp} = 8 \text{ meV}$ .  $m_e$  is the bare electron mass.

$E_{\text{exc},k} = \frac{\hbar^2 k^2}{2m_{\text{exc}}}$ ,  $E_{\text{ph},k} = \frac{\hbar^2 k^2}{2m_{\text{ph}}}$ , and  $g_{xp}$  is the magnitude of the vacuum Rabi splitting of the exciton energy due to the strong interaction with the band edge (which we choose to be at  $\vec{q} = 0$  for convenience) photon.  $g_{xp}$  determines the depth of the dressed exciton dispersion minimum. Figure 4 shows a typical dispersion curve with parameters chosen for excitons in a realistic PBG QW heterostructure.<sup>22</sup>

Figure 5 shows the critical temperature for dressed exciton condensation as a function of exciton density using Eqs. (18) and (17). The appearance of the bare exciton effective mass for large momentum deviation from the photonic band edge leads to a BEC critical transition temperature in the range of tens of Kelvin. We note that for the effective mass of the dressed exciton achievable in our photonic band gap structure, the curves are indistinguishable on the resolution scale of Fig. 5. If, on the other hand, we choose the dressed exciton effective mass that is artificially 100 times larger than that for Fig. 5,

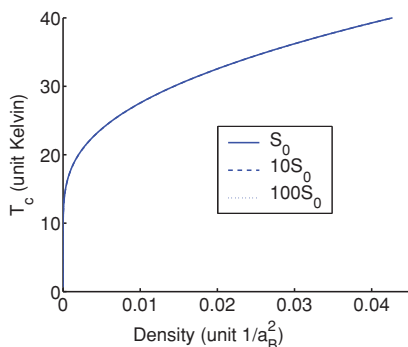


FIG. 5. (Color online) The critical (reference) temperature  $T_c$  for excitons dressed by band edge photons as a function of the particle density.  $T_c$  is defined by Eq. (17) with the assumption of zero occupation of the ground state for the dressed exciton at three different choices of exciton confinement area. Here  $S_0 = (10 \mu\text{m})^2$ , and the dispersion of the dressed exciton is given by Eq. (18) with parameters given in the caption of Fig. 4.

the effect of the larger confinement area would appear more visibly as leading to a larger critical density for BEC. In the present paper, we focus on 2D-box confinement. In this case the dispersion (18) is used and the exciton wave function is required to vanish along the boundaries of a fixed square region.

### B. Properties of the dressed exciton condensate

In Sec. III, we presented a detailed description of a single mode interacting boson model. However, the dispersion relation for excited bosons is required to describe the realistic spontaneous coherence buildup at low temperature. Here, we consider the complete model including the dressed exciton dispersion [Eq. (18)], and two equations (8) and (7) (for thermal and Poisson-like distributions, respectively) that connect the average ground state occupation with the true chemical potential. We study the conditions for Bose condensation and the nature of quantum statistics for various choices of temperature, trapping area, the strength of exciton-photon coupling, and exciton-exciton repulsion.

Defining the dimensionless variables  $\tilde{k} = k\frac{\sqrt{S}}{2\pi}$ ,  $E_{\text{exc}}^{\tilde{k}} = \frac{(2\pi\hbar)^2}{2m_{\text{exc}}S k_B T}$ ,  $E_{\text{ph}}^{\tilde{k}} = \frac{(2\pi\hbar)^2}{2m_{\text{ph}}S k_B T}$ ,  $\tilde{g}_{xp} = \frac{\hbar g_{xp}}{k_B T}$ , the dimensionless value of the dressed exciton realistic dispersion curve  $\epsilon_k$  given by Eq. (18) becomes  $\tilde{\epsilon}_{\tilde{k}} = \frac{E_{\text{exc}}^{\tilde{k}} + E_{\text{ph}}^{\tilde{k}} - \sqrt{(E_{\text{exc}}^{\tilde{k}} - E_{\text{ph}}^{\tilde{k}})^2 + 4\tilde{g}_{xp}^2}}{2} + \tilde{g}_{xp}$ . The dimensionless Bogoliubov elementary excitation energy is  $\tilde{\epsilon}_{\tilde{k}} = \sqrt{[\tilde{\epsilon}_{\tilde{k}} - \tilde{\mu} + (\tilde{g}_0 + \tilde{g}_k)N_0]^2 - (\tilde{g}_k N_0)^2}$ , where  $\tilde{\mu} = \tilde{g}_0 x_0 - \ln(1 + x_0^{-1})$ . Since the sign of the chemical potential is determined by the sign of  $\tilde{g}_0 x_0^2 - 1$ , combining Eqs. (7) and (8) and transforming the summation into integration, we obtain

$$N = N_0 + 2\pi \int \tilde{k} d\tilde{k} \left( \frac{\tilde{\epsilon}_{\tilde{k}} - \tilde{\mu} + (\tilde{g}_0 + \tilde{g}_k)N_0 - \tilde{\epsilon}_{\tilde{k}}}{2\tilde{\epsilon}_{\tilde{k}}} + \frac{\tilde{\epsilon}_{\tilde{k}} - \tilde{\mu} + (\tilde{g}_0 + \tilde{g}_k)N_0}{\tilde{\epsilon}_{\tilde{k}}(e^{\tilde{\epsilon}_{\tilde{k}}} - 1)} \right) \tilde{g}_0 x_0^2 > 1, \quad (19a)$$

$$N = N_0 + 2\pi \int \tilde{k} d\tilde{k} \frac{1}{e^{[\tilde{\epsilon}_{\tilde{k}} - \tilde{\mu} + (\tilde{g}_0 + \tilde{g}_k)N_0]} - 1} \tilde{g}_0 x_0^2 < 1. \quad (19b)$$

Here, to convert from summation to integral, the energy level spacing in our box should be less than the energy scale  $k_B T$ . For our typical choice of exciton confinement area  $S = (10 \mu\text{m})^2$ , this, strictly speaking, requires  $T \gtrsim 10 \text{ K}$ . For lower temperatures, a precise treatment requires that we retain eigenvalues in the range  $(0, \hbar g_{xp})$  as discrete terms in the summation. However, these terms are relatively small compared to the summation over higher energy states (with much larger bare-exciton effective-mass and energy spacing much less than  $k_B T$ ). As a result it is a reasonable approximation, for all temperatures, to replace all discrete terms (except the ground state) by an integral.

There are two primary quantities of interest. One is the condensate fraction,  $\frac{N_0}{N_{\text{tot}}}$  ( $N_{\text{tot}} \equiv N$ ). The other is the degree of second order of coherence in the ground state. We plot these two quantities as a function of temperature and exciton confinement area, both of which can be tuned *in situ*. Other parameters, such as the dressed exciton dispersion depth (i.e.,  $g_{xp}$ ) and the dressed exciton effective mass (both due to

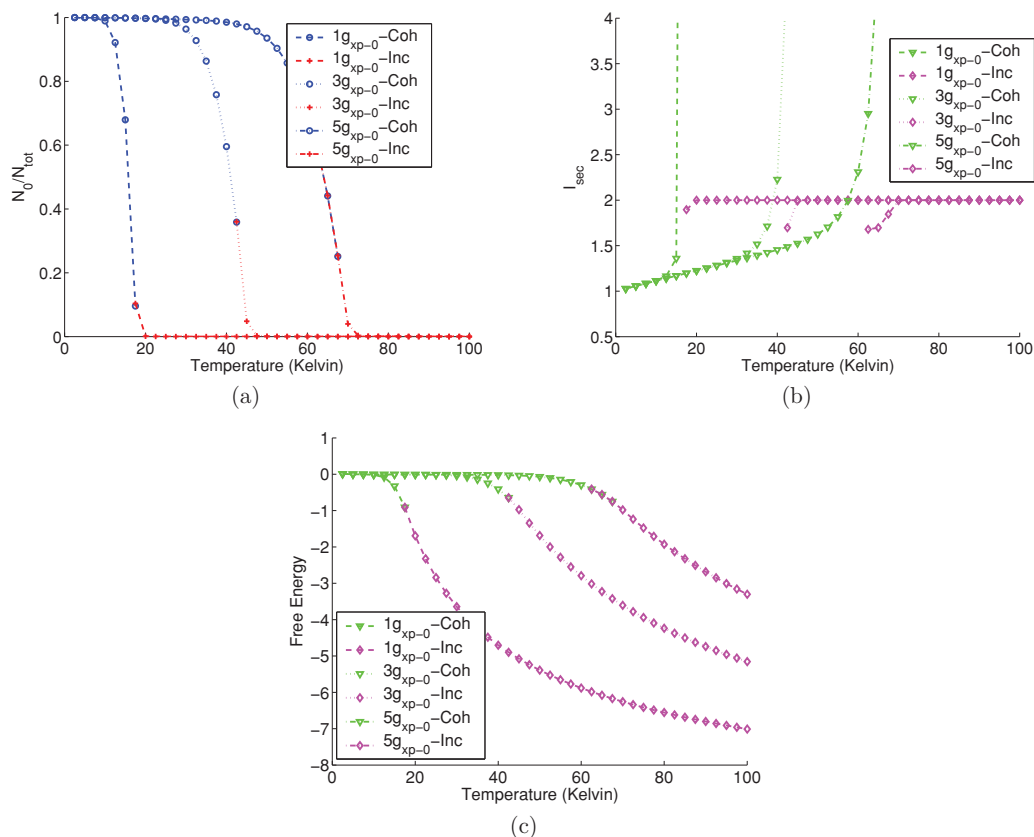


FIG. 6. (Color online) (a) The value of  $\frac{N_0}{N_{tot}}$  as a function of temperature for three different choices of strong exciton-photon coupling is shown. The parameters  $S_0$ ,  $g_0$ ,  $N_{tot-0}$ ,  $m_{exc-0}$ ,  $m_{ph-0}$ , and  $g_{xp-0}$  are defined below Eq. (19). (b) The degree of second order coherence and (c) the Helmholtz free energy defined by Eq. (20) are shown for each solution in (a). Three curves with circles (blue online and denoted by *Coh* in the legend) are obtained from the Eq. (19a) for the positive chemical potential. Their degrees of second order coherence are shown by three curves with triangle symbols (green online) in Fig. 6(b). The other three curves with plus symbols (red online and denoted by *Inc* in the legend) are obtained from Eq. (19b) for negative chemical potential and their degrees of second order coherence are three curves with diamonds (magenta online).

exciton-photon interaction), may be engineered to some extent as well. For concreteness, we use the following base parameters in the discussion below. The confinement area is  $S_0 = (10 \mu\text{m})^2$ , dressed exciton repulsive energy  $g_0 = 7.5 \text{ meV}$  and the total number of dressed excitons is  $N_{tot-0} = 1000$ . We also choose the exciton-photon coupling  $g_{xp-0} = 8 \text{ meV}$ , the bare exciton effective mass  $m_{exc-0} = 0.57m_e$  and band edge photon effective mass  $m_{ph-0} = 5.7 \times 10^{-6}m_e$  ( $m_e$  is bare electron mass) to specify the dressed exciton dispersion. Whenever these parameters are changed from these base values, a detailed description is provided in the figure caption.

In Fig. 6(a), below a critical temperature determined by the trap size, exciton density, and repulsive interaction, the system exhibits a crossover to a macroscopic occupation of the ground state with the chemical potential still negative [indicated by the curves with the plus symbol (red online)]. When the temperature decreases further, a self-consistent solution of Eq. (19b) based on negative chemical potential no longer exists. At a temperature below the BEC temperature, the only solution appears in the other branch described by Eq. (19a), [depicted in Fig. 6(a) by the curves with circle symbols (blue online)], based on a positive chemical potential. As the temperature decreases, the degree of second order

coherence decreases from 2 towards 1 [shown in Fig. 6(b) by the curves with diamond symbols (magenta online)] for negative chemical potential. It then jumps to a larger positive value [shown in Fig. 6(b) by the curves with triangle symbols (green online)] indicating large number fluctuations in the condensate at the transition from negative to positive chemical potential. At the temperature of this transition (chemical potential changes from negative to positive), there is no dramatic change in the overall distribution function and the expectation value of the number of ground state particles has no discontinuity. However, there is a slight change of the peak position from zero for negative potential to nonzero for positive potential. This indicates a larger probability to occupy high number states and a lower probability to occupy low number states. The fluctuation due to occupying lower number states is bounded, however, the fluctuation due to occupying larger number states is not bounded. This leads initially to a super-Poissonian distribution for the positive chemical potential with a much broader width than the expectation value of the ground state particles. In the positive chemical potential branch, the degree of second order of coherence then drops rapidly with temperature to below 1, indicating exciton antibunching in the condensate.

To determine the relative stability of the coherent and incoherent states, we consider the Helmholtz free energy for both solutions of Eqs. (19)

$$F = U - TS = -k_B T (\ln Z - \tilde{\mu} N_{\text{tot}}). \quad (20)$$

We use the following grand partition function for the generalized Bogoliubov model

$$Z = Z_0 \cdot Z_e \cdot Z_{\text{const}}, \quad (21a)$$

where

$$Z_e = \prod_{k \neq 0} \frac{1}{1 - e^{-\beta E_k}}, \quad (21b)$$

with

$$E_k = \begin{cases} \epsilon_k & : \tilde{g} x_0^2 < 1, \\ \epsilon_k & : \tilde{g} x_0^2 > 1, \end{cases} \quad (21c)$$

and

$$Z_{\text{const}} = e^{\beta H_{\text{const}}}. \quad (21d)$$

Here  $H_{\text{const}}$  is given by Eq. (3d),  $\epsilon_k$  is the bare exciton energy [Eq. (18)], and the Bogoliubov elementary excitation energy  $\epsilon_k = \sqrt{[\epsilon_k - \mu + (g_0 + g_k)N_0]^2 - (g_k N_0)^2}$ .  $Z_0$  is the grand partition function for the condensate given by Eq. (12). Since we take the limit as  $I_e$  and  $J_e$  approach zero when calculating  $Z_0$ , we set  $Z_{\text{const}} = 1$  for consistency.

If the exciton-photon coupling is made stronger, a deeper local minimum in the dressed exciton dispersion occurs and the critical temperature for BEC increases. In this case it is possible to observe an overlap region in the temperature between the two branches of thermodynamic equilibrium described in Eq. (19) [dash-dot curve with circles (blue online) and dash-dot curve with plus symbols (red online)]. This is most evident in Fig. 6(a) for the larger value ( $5g_{xp}$ ) exciton-photon coupling. In this overlap region, both Eqs. (19a) and (19b) exhibit a solution at the same temperature. Starting from a sub-Poissonian state

(blue curve) at a very low temperature, our model predicts a narrow region of bistability as the temperature approaches the BEC temperature from the condensate phase in which both partially coherent and incoherent solutions exist. As the temperature increases further, no solution exists for the positive chemical potential and the system transfers from the bistable state to the incoherent state.

Figure 6(c) shows the Helmholtz free energy for each state described in Fig. 6(a). Clearly the free energies are quite close for the incoherent and coherent states in the coexistence region. The detailed nature of the transition between these states may require a more precise treatment of the terms  $I_e$  and  $J_e$ .

Figure 7 illustrates the role of the exciton-exciton repulsive interaction on BEC and exciton statistics within the condensate. The system starts to have a macroscopic number of particles in the ground state while the chemical potential is still negative as indicated by the curves with plus symbols (red online). As the temperature drops further below the BEC critical temperature, no more self-consistent solution of Eq. (19b) based on the negative chemical potential exists. The system switches to the positive chemical potential solution Eq. (19a) [curves with circles (blue online)]. Unlike the variation of the exciton-photon coupling  $g_{xp}$ , the variation of exciton-exciton coupling has a minor influence on the BEC critical temperature. However, we are able to observe a larger overlap region in temperature (where coherent and incoherent solutions coexist) for smaller exciton-exciton repulsive interaction [indicated by the dash-dot curve with circles (blue online) and the dash-dot curve with plus symbols (red online) in Fig. 7(a)].

In Fig. 8, we consider the role of the dressed-exciton effective mass on BEC and condensate statistics. As the effective mass becomes larger, the critical BEC temperature decreases as indicated by the shift of curves for  $N_0/N_{\text{tot}}$  to the left. To bring the BEC temperature back to order of tens

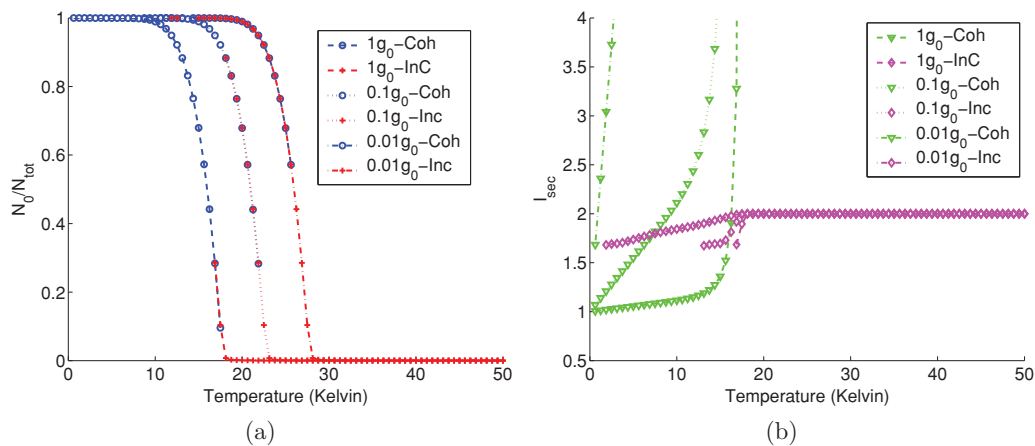


FIG. 7. (Color online) (a) The value of  $\frac{N_0}{N_{\text{tot}}}$  as a function of temperature for three different choices of exciton-exciton coupling is shown. The parameters  $S_0$ ,  $g_0$ ,  $N_{\text{tot}-0}$ ,  $m_{\text{exc}-0}m_{\text{ph}-0}$ , and  $g_{xp-0}$  are defined below Eq. (19). (b) The degree of second order coherence for each solution in (a) is shown. Three curves with circles (blue online and denoted by *Coh* in the legend) are obtained from Eq. (19a) for positive chemical potential, their degrees of second order coherence are shown by three curves with triangle symbols (green online) in (b). The other three curves with plus symbols (red online and denoted by *Inc* in the legend) are obtained from Eq. (19b) for negative potential and their degrees of second order coherence are three curves with diamonds (magenta online). Since the exciton-exciton repulsive interaction has no significant influence on the BEC critical temperature, all curves in (a) for different exciton-exciton interaction are in overlap. For the sake of visual clarity, we artificially shift the curve in (a) for  $0.1g_0$ , 5 K toward the right part of the figure, and we shift the curve for  $0.01g_0$ , 10 K toward the right.

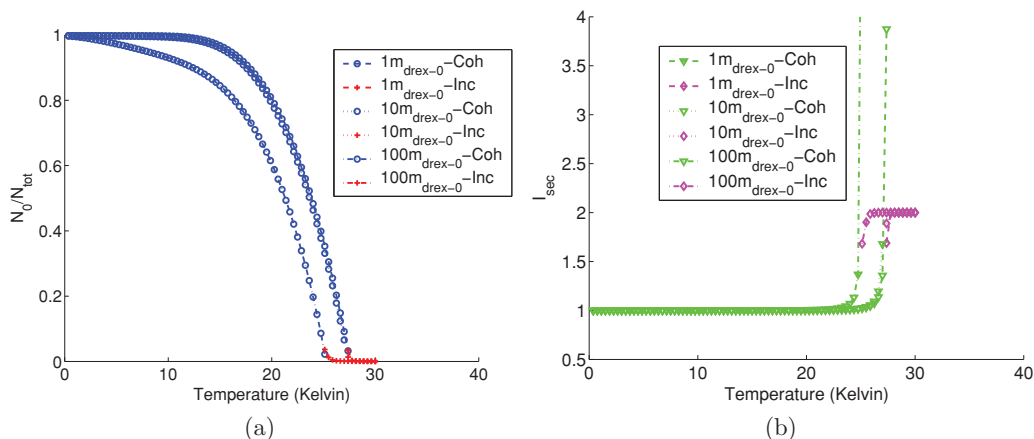


FIG. 8. (Color online) (a) The value of  $\frac{N_0}{N_{\text{tot}}}$  as a function of temperature for three different choices of dressed exciton effective mass is shown. The parameters  $S_0, N_{\text{tot}} = 10N_{\text{tot-0}}$ ,  $m_{\text{exc-0}} = m_{\text{ph-0}}$ , and  $g_{xp-0}$  are defined below Eq. (19). (b) The degree of second order coherence for each solution in (a) is shown. Here  $m_{\text{drex-0}}$  in the legend denotes the effective mass of the dressed exciton. We obtain  $m_{\text{drex-0}} \approx 2m_{\text{ph-0}}$  from Eq. (18) for the case  $m_{\text{exc}} \gg m_{\text{ph}}$ . Three curves with circles (blue online denoted by *Coh* in the legend) are obtained from Eq. (19a) for the positive chemical potential. Their degrees of second order coherence are shown by three curves with triangle symbols (green online) in (b). The other three curves with plus symbols (red online and denoted by *Inc* in the legend) are obtained from Eq. (19b) for the negative potential and their degrees of second order coherence are three curves with diamonds (magenta online).

of Kelvin, we make an additional parameter change, setting  $N_{\text{tot}} = 10^4$ , for all three-different choices of dressed-exciton effective mass in Fig. 8. As the temperature decreases, we observe the change of ground state statistics from thermal to Poissonian. The system with large effective mass has a higher density of low energy excited states. This leads to a lower condensate fraction at a given temperature. However, the coexistence region in temperature with two branches of solutions disappears for large effective mass.

A system with large effective mass is able to accept more particles in lower energy excited states than one with small effective mass. When the temperature is below the critical temperature, even a small condensate fraction means a large number of particles are in the ground state. This increases the ground state interaction energy (i.e.,  $g_0 N_0^2/2$ ). The transition in exciton quantum statistics is determined by the sign of  $\tilde{g}_0 N_0^2 - 1$  [see discussion above Eq. (15)]. Therefore, the ground state particles will easily become Poissonian distributed once the temperature is less than BEC critical temperature. Applying Eq. (17) to bare bosons with effective mass  $m_{\text{eff}}$  in a 2D-box potential, we have  $N \sim y_c \ln y_c$ , where  $y_c = \frac{2m_{\text{eff}} S k_B T_c}{(\hbar\pi)^2}$ . Fixing  $N$  and using Eq. (16) with  $z \simeq 1$ , we have  $N_0 = N - N_e \sim y_c \ln y_c - y \ln y \simeq (y_c - y) \ln y_c$  where  $y = \frac{2m_{\text{eff}} S k_B T}{(\hbar\pi)^2}$ . For small positive  $T_c - T$ , we obtain

$$N_0 \sim N \frac{T_c - T}{T_c} \quad (\text{for } T \lesssim T_c). \quad (22)$$

The coexistence of two solutions below the BEC transition is the result of persistence of the incoherent state ( $\tilde{\mu} < 0$ ) for  $T \lesssim T_c$ . This persistence is, in turn, defined by the condition  $\tilde{g}_0 N_0^2 = 1$ . Substituting Eq. (22) into this condition and approximating  $\tilde{g}_0 \simeq g_0/(k_B T_c)$ , we arrive at secondary temperature scale  $T_*$  for the disappearance of the incoherent solution

$$\frac{T_c - T_*}{T_c} \simeq \frac{k_B T_c}{N g}. \quad (23)$$

The temperature range of the potential incoherence below  $T_c$  defined by Eq. (23) increases with a smaller repulsive interaction. It also increases with a smaller effective mass and smaller confinement area through the dependence of  $T_c$  [on the right-hand side of Eq. (23)] of these two parameters.

Figure 9(a) shows the effect of the exciton confinement area on Bose condensation and exciton statistics. A smaller confinement area enables BEC at higher temperature. If the confinement area is decreased at a fixed temperature, a macroscopic occupation of the ground state is initiated while the chemical potential is still negative [indicated by the curves with plus symbols (red online)]. As the confinement area decreases further, a self-consistent solution from Eq. (19b) based on the negative chemical potential no longer exists. The system then switches to the solution of Eq. (19a) based on the positive chemical potential. As before, the degree of second order coherence initially decreases with a smaller confinement area for the negative chemical potential, but then jumps when switching from negative to positive chemical potential. The degree of second order coherence then decreases precipitously as the confinement area is made smaller.

At zero temperature with repulsive exciton-exciton interaction, all excitations do not simply condense into a fixed number state. Interaction induces some occupation of single-particle excited states. This is reflected in the nonzero expectation values of the following quantities:

$$N_e = \sum_{k \neq 0} \langle a_k^+ a_k \rangle = \sum_{k \neq 0} \frac{\epsilon_k - \mu + (g_0 + g_k) N_0 - \epsilon_k}{2\epsilon_k}, \quad (24a)$$

$$|J_e| = \left| \frac{1}{2} \sum_{k \neq 0} g_k \langle a_k^+ a_{-k}^+ \rangle \right| = \frac{1}{2} \sum_{k \neq 0} g_k \frac{g_k N_0}{2\epsilon_k}. \quad (24b)$$

Figure 10 depicts  $\frac{N_e}{N_0}$  and  $\frac{|J_e|}{g_0 N_0}$  as a function of the number of particles in the ground state at zero temperature. As a result

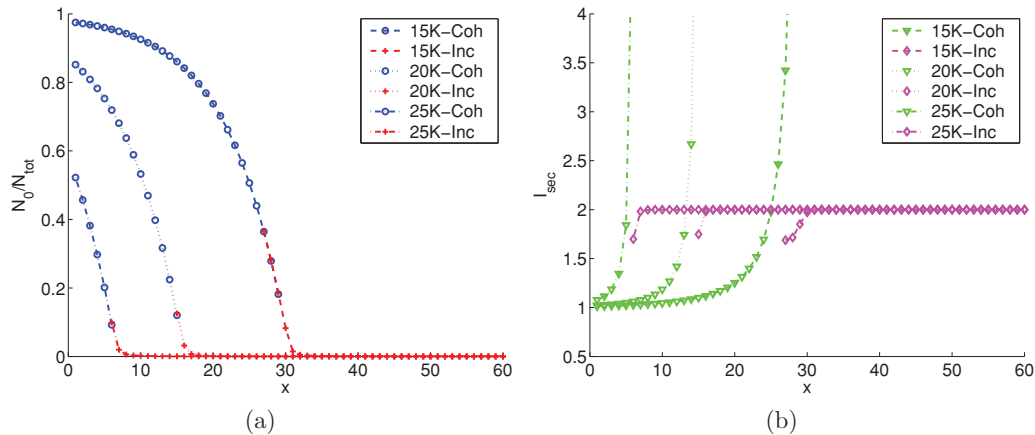


FIG. 9. (Color online) (a) shows the value of  $\frac{N_0}{N_{\text{tot}}}$  as a function of exciton confinement area  $S$  for three different choices of temperature, where  $x = 8 \cdot (\ln(S/S_0) + 2.697)$ . The other parameters are  $S_0, N_{\text{tot}-0}, m_{\text{exc}-0}, m_{ph-0}$ , and  $g_{xp-0}$  defined below Eqs.(19). (b) shows the degree of second order coherence for each solution in (a). Three curves with circles (blue online and denoted by *Coh* in legend) are obtained from Eq. (19a) for positive chemical potential. Their degrees of second order coherence are shown by three curves with triangle dots (green online) in (b). The other three curves with plus symbols (red online and denoted by *Inc* in legend) are obtained from Eq. (19b) for negative potential and their degrees of second order coherence are three curves with diamonds (magenta online).

of the repulsive exciton-exciton interaction, some excitons occupy nonzero wave vector states even for  $T = 0$ . As the confinement area decreases, the dressed exciton repulsive interaction is effectively increased and more particles are forced into nonzero wave vector states. The nonzero magnitude of  $J_e$  is important to drive exciton coherence by introducing nondiagonal coupling in the condensate as shown in Eq. (3c). In the absence of such an interaction, the statistical distribution of excitons in the ground state would be a pure number state.

## V. CONCLUSION

We have presented a model for the equilibrium quantum statistics of a condensate of repulsively interacting bosons in a two-dimensional trap. Unlike the standard Bogoliubov<sup>2</sup> treatment that assumes coherent state formation (Poissonian number distribution) in the ground state, we consider particle correlations in the condensate exactly using a quantum anhar-

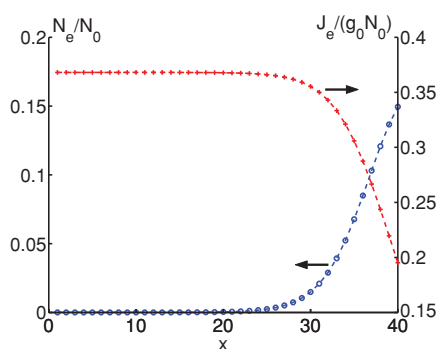


FIG. 10. (Color online) The value of  $\frac{N_e}{N_0}$  and  $\frac{|J_e|}{g_0 N_0}$  as a function of ground state (at zero wave vector) particle number ( $N_0$ ) at zero temperature. Here, the horizontal axis is  $x = \ln(N_0)/0.375$ . The other parameters used,  $S_0, m_{\text{exc}-0}, m_{ph-0}$ , and  $g_{xp-0}$  are defined below Eq. (d19).

monic oscillator model. The quantum statistical distribution of particles in the condensate is determined by the sign of the chemical potential relative to the zero-point energy  $\epsilon_0 - g_0/2$ , where  $g_0$  is the repulsion energy of ground state dressed excitons. The sign of the chemical potential, in turn, is qualitatively determined by the value of the dimensionless parameter  $\frac{g_0 N_0^2}{k_B T}$  relative to unity, where  $N_0$  is the number of particles in the single-particle ground state. When this parameter exceeds unity, the number distribution has a nonzero peak, otherwise the condensate exhibits a monotonic number distribution. Unlike traditional Bogoliubov theory in which a coherent ground state is assumed, our exact treatment of condensate particle correlations is used to connect the chemical potential to the condensate fraction and then derive physical quantities involving the resulting excitation spectrum. As a result of this more exact treatment we find that the chemical potential undergoes a jump (in mean-field theory) between a monotonic exciton distribution and a partially coherent one at a temperature just below the BEC critical temperature. As the temperature is lowered further, the condensate exhibits more coherence and eventually sub-Poissonian fluctuations. We focus on two physical properties, the condensate fraction and the degree of second order coherence of Bose condensed excitons as a function of temperature and confinement area for various choices of the exciton-photon coupling constant, the exciton-exciton repulsion, and the dressed exciton effective mass. Some common features appear for decreasing temperature. The interacting Bose system exhibits a macroscopic occupation of the single-particle ground state below a critical temperature, and its degree of second order coherence decreases from 2 (a typical value for thermal distributed bosons) to 1 with decreasing temperature. This is facilitated by a switching between two distinct mean-field solutions at a temperature slightly below the onset of BEC. Decreasing temperature below the switching point, the number distribution of condensate particles evolves from super-Poissonian to Poissonian and then to sub-Poissonian.

The particle number fluctuations become smaller and smaller, and the statistical distribution exhibits antibunching, with the degree of second order coherence slightly below unity. We find that decreasing the exciton-confinement area has a similar effect to decreasing temperature. A striking feature of our mean-field theory is the coexistence region (in temperature), where two branches of solutions (one partially coherent and the other incoherent) occur for a large exciton-photon coupling, weak exciton-exciton repulsive interaction, and ultrasmall effective mass.

Our model provides a starting point for a more precise self-consistent mean-field treatment of the quantum expectation value  $J_e$  associated with bosons excited out of the single particle ground state. This may lead to further quadrature squeezing<sup>25</sup> of the condensate. Nevertheless, our model suggests that an excitonic condensate in a PBG-quantum well may serve as a novel tunable source for nonclassical states of light through the control of exciton quantum statistics. Nonclassical light emission from the condensate may be induced through a rapid switching of the photonic band edge relative to the exciton radiative emission frequency. Band edge frequency shifts have been demonstrated in a variety of tunable photonic crystals.<sup>31,32</sup> If the excitonic condensate is suddenly switched into a regime of very high electromagnetic density of states at the recombination frequency and the switching time scale is short compared to the new equilibrium time scale of the emitted photons, nonclassical emission may be observable.

#### ACKNOWLEDGMENTS

This work was supported in part by the Natural Science and Engineering Research Council of Canada and the Canadian Institute for Advanced Research.

#### APPENDIX: EVALUATION OF THE PARTITION FUNCTION FOR SINGLE MODE BOSON MODEL WITH REPULSIVE INTERACTION

To evaluate the partition function (10), we introduce the integral representation  $e^{-\frac{1}{2}\tilde{g}n^2} = \sqrt{\frac{\tilde{g}}{2\pi}} \int_{-\infty}^{+\infty} dx [e^{-\frac{1}{2}\tilde{g}(x^2-2ixn)}]$ . Then,

$$\begin{aligned} Z &= \sqrt{\frac{\tilde{g}}{2\pi}} \int_{-\infty}^{+\infty} dx \left[ e^{-\frac{1}{2}\tilde{g}x^2} \sum_n e^{(\tilde{\mu}+i\tilde{g}x)n} \right] \\ &= \lim_{N \rightarrow \infty} \sqrt{\frac{\tilde{g}}{2\pi}} \int_{-\infty}^{+\infty} dx \left[ e^{-\frac{1}{2}\tilde{g}x^2} \frac{e^{(\tilde{\mu}+i\tilde{g}x)N} - 1}{e^{(\tilde{\mu}+i\tilde{g}x)} - 1} \right]. \end{aligned} \quad (\text{A1})$$

Provided  $\text{Re}(\tilde{\mu} + i\tilde{g}x) < 0$ , the limit is well defined and we can analytically continue the integrand to the whole complex plane except at the singularity  $ix_s (x_s = \frac{\tilde{\mu}}{\tilde{g}})$

$$Z = \sqrt{\frac{\tilde{g}}{2\pi}} \int_{-\infty}^{+\infty} dx [e^{-f(x)}], \quad (\text{A2})$$

where

$$f(x) = \frac{1}{2}\tilde{g}x^2 + \ln[1 - e^{\tilde{\mu}+i\tilde{g}x}].$$

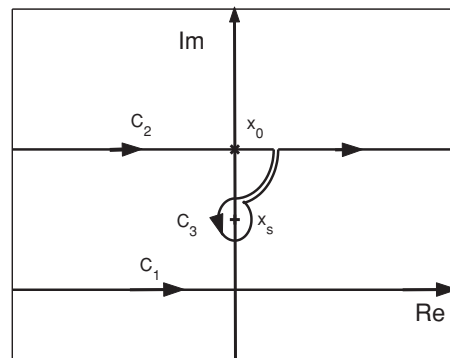


FIG. 11. Schematic diagram for deforming the original integration along the real axis for Eq. (A2) (i.e., the contour  $C_1$ ) to the integration along the solid line passing through the saddle point  $x_0$  (denoted by the contour  $C_2$ ), with additional residue from the contour  $C_3$  around the singularity  $x_s$ .

The integrand has a saddle point on the imaginary axis at  $ix_0$  defined by

$$f'(ix_0) = 0 = i\tilde{g}x_0 - \frac{i\tilde{g}e^{\tilde{\mu}-\tilde{g}x_0}}{1 - e^{\tilde{\mu}-\tilde{g}x_0}}. \quad (\text{A3})$$

Equivalently, the saddle point occurs when

$$\tilde{\mu} = \tilde{g}x_0 - \ln\left(1 + \frac{1}{x_0}\right). \quad (\text{A4})$$

In Fig. 11, as we shift the contour  $C_1$  of integration from  $(-\infty, +\infty)$  to the contour  $C_2(-\infty + ix_0, +\infty + ix_0)$  that passes through the saddle point, a singularity is crossed at  $x_s = \frac{i\tilde{\mu}}{\tilde{g}}$  if  $\tilde{\mu} > 0$ . In this case, we must include the residue contribution,  $Z_s$ , of the singularity from the contour  $C_3$  when using the steepest descent contour

$$Z = \begin{cases} Z_n & : \tilde{\mu} < 0, \\ Z_n + Z_s & : \tilde{\mu} > 0, \end{cases} \quad (\text{A5a})$$

$$Z_n = \sqrt{\frac{\tilde{g}}{2\pi}} \int_{-\infty}^{+\infty} dx [e^{-f(x+ix_0)}], \quad (\text{A5b})$$

$$f(x + ix_0) = \frac{1}{2}\tilde{g}(x + ix_0)^2 + \ln\left[1 - \frac{x_0}{1 + x_0} e^{i\tilde{g}x}\right], \quad (\text{A5c})$$

$$Z_s = \sqrt{\frac{\tilde{g}}{2\pi}} e^{\frac{1}{2}\frac{\tilde{\mu}^2}{\tilde{g}}} \frac{2\pi}{\tilde{g}}. \quad (\text{A5d})$$

Performing the second order Taylor expansion  $f(x) \approx f(0) + \frac{1}{2}f''(0)x^2$ , where  $f(0) = -\frac{1}{2}\tilde{g}x_0^2 - \ln[1 + x_0]$  and  $f''(0) = \tilde{g} + \tilde{g}^2(x_0 + x_0^2)$ . We obtain the saddle point approximation  $Z_n \simeq Z_A$ , where

$$Z_A = e^{\frac{1}{2}\tilde{g}x_0^2 + \ln[1+x_0]} [1 + \tilde{g}x_0(1 + x_0)]^{-1/2}. \quad (\text{A6})$$

Equation (A6) provides an estimate of  $Z_n$  under the saddle point approximation. However, the exact integral given by Eq. (A5b) is convergent. While the main contribution to  $Z_n$  is centered around  $x_0$ , it is straightforward to evaluate the correction to the saddle point approximation by numerical means. For this we write

$$Z_n = \sqrt{\frac{\tilde{g}}{2\pi}} \int_{-\infty}^{+\infty} dx \{e^{-[f(0)+f(x)-f(0)]}\}. \quad (\text{A7})$$

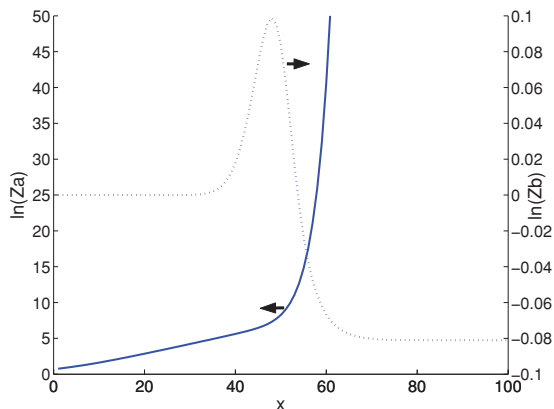


FIG. 12. (Color online) The value of  $\ln(Z_A)$  in the solid curve and  $\ln(Z_B)$  in dotted curve as a function of the saddle point  $x_0$  defined by Eq. (A4) for a typical case of  $\tilde{g}$  [ $S = (10 \mu\text{m})^2$ ,  $T = 25 \text{ K}$ ,  $g = 7.5 \text{ meV}$ ]. Here  $x = (\ln x_0)/0.15$ . The variation of  $\ln(Z_B)$  is much less than the variation of  $\ln(Z_A)$  in the whole range of  $x_0$ . The curve of  $\ln Z_A + \ln Z_B$  is monotonically increasing. The exact solution  $x_0$  for a given  $N_0$  is shifted slightly due to the additional term  $\ln Z_B$ . The maximum error of the first order derivative of  $\ln Z$  (caused by neglecting  $\ln Z_B$ ) is about 8% at the position  $x = 45$  ( $\tilde{g}x_0^2 = 1$ ). In addition, for the case of  $\tilde{\mu} > 0$ , the large weighting of  $Z_s$  further decreases the error caused by neglecting  $\ln Z_B$ .

It is straightforward to show that  $Z_n = Z_A Z_B$ , where

$$\begin{aligned} Z_B &= \left[ \frac{f''(0)}{2\pi} \right]^{1/2} \int_{-\infty}^{+\infty} dx \frac{e^{-(\frac{1}{2}\tilde{g}x^2 + i\tilde{g}xx_0)}}{1 + x_0 - x_0 e^{i\tilde{g}x}} \\ &= \sqrt{\frac{2}{\pi}} \int_0^{+\infty} dx \text{Re} \left[ \frac{\sqrt{\tilde{g} + \tilde{g}^2(x_0^2 + x_0)}}{1 + x_0 - x_0 e^{i\tilde{g}x}} e^{-\frac{1}{2}\tilde{g}x^2 - i\tilde{g}xx_0} \right]. \end{aligned} \quad (\text{A8})$$

$$\frac{\partial \langle N_0 \rangle}{\partial \tilde{\mu}} = \begin{cases} N_n^{(1)} = Q_n^{(1)}(x_0^{(1)})^2 + Q_n x_0^{(1)} x_0^{(2)} & : \tilde{g}x_0^2 < 1, \\ W_s N_s^{(1)} + W_n N_n^{(1)} + W_s W_n (N_s - N_n)^2 & : \tilde{g}x_0^2 > 1, \end{cases} \quad (\text{A10a})$$

$$Q_n^{(1)} = \left( \tilde{g} - \frac{1}{(1+x_0)^2} - \frac{\tilde{g}}{1+\tilde{g}x_0^2} + \frac{2(\tilde{g}x_0)^2}{(1+\tilde{g}x_0^2)^2} \right), \quad (\text{A10b})$$

$$x_0^{(2)} = \frac{1+2x_0}{[1+\tilde{g}(x_0+x_0^2)]^2}, \quad (\text{A10c})$$

where  $N_s^{(1)} = 1/\tilde{g}$  and  $N_n \equiv \ln Z_n / \partial \tilde{\mu}$ .

The solid line and dashed line in Fig. 12 show the values of  $\ln Z_A$  and  $\ln Z_B$  for a typical value of  $\tilde{g}$ . In general  $\ln Z_B$  exhibits a peak around the value of  $\tilde{g}x_0^2 = 1$ , but approaches constants for both large and small  $\tilde{g}x_0^2$ . The quantities of physical interest are related to derivatives of  $\ln Z$ . Clearly, the derivative of  $\ln Z_B$  is much smaller than  $\ln Z_A$ . This justifies our use of the saddle point approximation  $Z_n \simeq Z_A$ .

The expectation value of the number of particles in the ground state is

$$\langle N_0 \rangle = \frac{\partial}{\partial \tilde{\mu}} \ln Z = \begin{cases} Q_n x_0^{(1)} & : \tilde{\mu} < 0, \\ W_s N_s + W_n Q_n x_0^{(1)} & : \tilde{\mu} > 0, \end{cases} \quad (\text{A9a})$$

where

$$Q_n = \frac{\partial \ln Z_n}{\partial \tilde{\mu}} = \frac{1}{1+x_0} + \frac{(\tilde{g}x_0)^2 x_0}{1+\tilde{g}x_0^2}, \quad (\text{A9b})$$

$$x_0^{(1)} \equiv \frac{\partial x_0}{\partial \tilde{\mu}} = \frac{x_0 + x_0^2}{1+\tilde{g}(x_0+x_0^2)}, \quad (\text{A9c})$$

$$W_s = 1 - W_n = \frac{Z_s}{Z_n + Z_s}, \quad (\text{A9d})$$

$$N_s \equiv \frac{\partial \ln Z_s}{\partial \tilde{\mu}} = \frac{\tilde{\mu}}{\tilde{g}} = x_0 - \frac{1}{\tilde{g}} \ln \left( 1 + \frac{1}{x_0} \right). \quad (\text{A9e})$$

For a given average particle number  $\langle N_0 \rangle$  in the ground state, we can solve for  $x_0$  in Eq. (A9) and obtain the chemical potential through the relation (A4). In addition, the evaluation of the degree of second order coherence, that is, Eq. (14) requires  $\frac{\partial \langle N_0 \rangle}{\partial \tilde{\mu}}$  which is obtained from Eq. (A9) and described by

\*john@physics.utoronto.ca

<sup>1</sup>A. Einstein, Sitz. Ber. Preuss. Akad. Wiss. **23**, 3 (1925).

<sup>2</sup>N. N. Bogoliubov, J. Phys. (USSR) **11**, 23 (1947).

<sup>3</sup>H. Deng, G. Weihs, D. Snoke, J. Bloch, and Y. Yamamoto, Proc. Natl. Acad. Sci. **100**, 15318 (2003).

<sup>4</sup>R. Balili, V. Hartwell, D. Snoke, L. Pfeiffer, and K. West, Science **316**, 1007 (2007).

<sup>5</sup>M. H. Anderson, J. R. Ensher, M. R. Matthews, C. E. Wieman, and E. A. Cornell, Science **269**, 198 (1995).

<sup>6</sup>K. B. Davis, M. O. Mewes, M. R. Andrews, N. J. van Druten, D. S. Durfee, D. M. Kurn, and W. Ketterle, Phys. Rev. Lett. **75**, 3969 (1995).

<sup>7</sup>F. Tassone, C. Piermarocchi, V. Savona, A. Quattropani, and P. Schwendimann, Phys. Rev. B **56**, 7554 (1997).

- <sup>8</sup>F. Tassone and Y. Yamamoto, *Phys. Rev. B* **59**, 10830 (1999).
- <sup>9</sup>G. Malpuech, A. Kavokin, A. Di Carlo, and J. J. Baumberg, *Phys. Rev. B* **65**, 153310 (2002).
- <sup>10</sup>D. Porras, C. Ciuti, J. J. Baumberg, and C. Tejedor, *Phys. Rev. B* **66**, 085304 (2002).
- <sup>11</sup>T. D. Doan, H. T. Cao, D. B. Tran Thoai, and H. Haug, *Phys. Rev. B* **72**, 085301 (2005).
- <sup>12</sup>D. Sarchi and V. Savona, *Phys. Rev. B* **75**, 115326 (2007).
- <sup>13</sup>F. P. Laussy, G. Malpuech, A. Kavokin, and P. Bigenwald, *Phys. Rev. Lett.* **93**, 016402 (2004).
- <sup>14</sup>P. Schwendimann and A. Quattropani, *Phys. Rev. B* **74**, 045324 (2006).
- <sup>15</sup>H. Deng, G. Weihs, C. Santori, J. Bloch, and Y. Yamamoto, *Science* **298**, 199 (2002).
- <sup>16</sup>M. H. Szymańska, J. Keeling, and P. B. Littlewood, *Phys. Rev. Lett.* **96**, 230602 (2006).
- <sup>17</sup>M. Wouters and I. Carusotto, *Phys. Rev. Lett.* **99**, 140402 (2007).
- <sup>18</sup>K. V. Kavokin, I. A. Shelykh, A. V. Kavokin, G. Malpuech, and P. Bigenwald, *Phys. Rev. Lett.* **92**, 017401 (2004).
- <sup>19</sup>J. Keeling, P. R. Eastham, M. H. Szymanska, and P. B. Littlewood, *Phys. Rev. B* **72**, 115320 (2005).
- <sup>20</sup>H. Deng, H. Haug, and Y. Yamamoto, *Rev. Mod. Phys.* **82**, 1489 (2010).
- <sup>21</sup>S. John and S. Yang, *Phys. Rev. Lett.* **99**, 046801 (2007).
- <sup>22</sup>S. Yang and S. John, *Phys. Rev. B* **75**, 235332 (2007).
- <sup>23</sup>C. Weisbuch, M. Nishioka, A. Ishikawa, and Y. Arakawa, *Phys. Rev. Lett.* **69**, 3314 (1992).
- <sup>24</sup>C. Ciuti, V. Savona, C. Piermarocchi, A. Quattropani, and P. Schwendimann, *Phys. Rev. B* **58**, 7926 (1998).
- <sup>25</sup>D. F. Walls and G. J. Milburn, *Quantum Optics* (Springer, Berlin, 1994).
- <sup>26</sup>B. Yurke and D. Stoler, *Phys. Rev. Lett.* **57**, 13 (1986).
- <sup>27</sup>V. Bužek, A. Vidiella Barranco, and P. L. Knight, *Phys. Rev. A* **45**, 6570 (1992).
- <sup>28</sup>C. M. Bender and T. T. Wu, *Phys. Rev.* **184**, 1231 (1969).
- <sup>29</sup>C. M. Bender and T. T. Wu, *Phys. Rev. D* **7**, 1620 (1973).
- <sup>30</sup>W. Ketterle and N. J. van Druten, *Phys. Rev. A* **54**, 656 (1996).
- <sup>31</sup>K. Busch and S. John, *Phys. Rev. Lett.* **83**, 967 (1999).
- <sup>32</sup>A. Forchel, *Nat. Mater.* **2**, 13 (2003).